# Super-stability splitting at the inhibition of the zeroth order by an encapsulated grating

ZHISEN HUANG, BO WANG*, ZEFAN LIN, KUNHUA WEN, ZIMING MENG, ZHAOGANG NIE, FANGTENG ZHANG, XIANGJUN XING, LI CHEN, LIANG LEI, JINYUN ZHOU
*School of Physics and Optoelectronic Engineering, Guangdong University of Technology, Guangzhou 510006, China*

A two-port encapsulated grating is proposed, whose zeroth order can be inhibited under normal incidence. The efficiencies of the ±1st orders can be more than 47% and 0th order can be less than 4% for both TE and TM polarizations at a bandwidth of 31 nm, from 1532 nm to 1563 nm. In addition, the fabrication tolerance is astonishingly good, where the efficiencies of greater than 47% can be satisfied in the ±1st orders within the period of 2914-3015 nm or the duty cycle of 0.290-0.458. The performance has important application value in optical communication, optical storage, etc.

(Received December 31, 2020; accepted October 7, 2021)

*Keywords:* Encapsulated grating; Inhibition of the zero order; Two-port beam splitter

## 1. Introduction

Beam splitting elements [1-6] play a key role in many optical fields with the characteristics of high efficiency, small volume and easy integration, which can be well applied in laser system [7-10], polarization imaging [11, 12], waveguide [13-16], optical communication system [17, 18] and so on. The grating can perform different functions at different incident angles such as normal incidence [19], second Bragg incidence [20] and Littrow incidence [21]. In the reported research, a variety of two-port beam splitting gratings with high performance have been designed. Most of these gratings [22-25] achieve two-port output in 0th order and -1st order under Littrow incidence. As for normal incidence, the grating can realize two-port output in ±1st orders with the inhibition of the zero order for both TE and TM polarization. This kind of grating has great value in many optical devices or systems. Wang et al. proposed a low-contrast transmission grating and a mixed metal reflective grating under normal incidence [26, 27]. For the transmission grating, the efficiency of ±1st orders under TE and TM polarizations are not high enough for the grating with 2nd order. The bandwidth performance of the reflective grating is not so good. Fu et al. designed a two-port reflective grating [28], whose bandwidth performance and fabrication tolerance are not so satisfactory. Yin et al. proposed a two-port metal-dielectric grating under normal incidence [29] at the incident wavelength of 800 nm.

When the grating period is equal to the wavelength, the optical device designed by scalar diffraction theory will lack reliability due to the obvious polarization characteristics of the grating. The vector diffraction theory about grating includes finite element method (FEM) [30], rigorous coupled-wave analysis (RCWA) [31] and so on. RCWA can expand the field distribution inside the grating according to Fourier, and then use the expression of eigenvalue and intrinsic field to analyze the relationship between the upper and lower boundary surface electromagnetic fields. Therefore, RCWA can be used to analyze gratings with any plane shape and any refractive index. In this paper, the design and optimization of grating are based on RCWA. At the same time, the electric field distribution [32] of the grating is calculated by FEM to better understand the performance of the grating.

In this work, a super-stability high-efficiency encapsulated grating is designed by RCWA. The structure of the encapsulated grating is different from that in Refs. [26-29], and the specific comparison is shown in Table 1. On the one hand, the proposed grating can uniformly couple the energy of the incident light to the ±1st orders for both TE and TM polarizations with the efficiency of greater than 48%. On the other hand, the efficiency of 0th order has been

well suppressed, which is less than 1% under TE and TM polarizations. Moreover, the grating performs surprisingly well in terms of bandwidth and fabrication tolerance.

*Table 1. Comparison of grating structure between this work and reported Refs. [26-29]*

| Grating structure | Ref. [26] | Ref. [27] | Ref. [28] | Ref. [29] | This work |
|---|---|---|---|---|---|
| Covering layer | No | No | No | Yes | Yes |
| Reflective layer | No | Yes | Yes | Yes | Yes |
| Connecting layer | No | No | Yes | Yes | No |

## 2. Physical design and numerical calculation

The structure of the two-port encapsulated grating with the inhibition of the zeroth order is shown in Fig. 1. As can be seen from Fig. 1, the grating is composed of four layers which are covering layer, grating layer (consists of grating ridge and grating groove), reflective layer and grating substrate. The covering layer, grating ridge and grating substrate are composed of fused silica with the refractive index $n_2$=1.45, and $h_g$ is the depth of the grating groove (the refractive index is $n_1$=1.00), where the material is air. The reflecting layer is made of silver with the refractive index $n_m$=0.469-i*9.32 and the thickness is $h_m$=0.100 μm. Moreover, d indicates as the grating period, $h_c$ is the thickness of the covering layer, b refers as the width of the grating ridge, and f represents as the duty cycle (defined as f=b/d). Above the covering layer is the incident region composed of air, in which a beam of light is incident at normal angle (the incidence angle is θ=0).

In this work, the fast selection and optimization of grating parameters and the calculation of diffraction efficiency are accomplished by RCWA. The associated electromagnetic conditions are shown below [31]. The optimal grating structure with parameters of d=2954 nm, f=0.43, $h_c$=1.190 μm and $h_g$=1.050 μm is obtained by the simulation of RCWA. The thickness of covering layer will affect the propagation of the incident light in the grating, while the etch depth of the grating groove will directly affect the phase difference of the coupled light wave. Figure 2 presents the relationship between reflection efficiency and the thickness of covering layer together the depth of grating groove under normal incidence. As illustrated in Fig. 2, when the thickness of covering layer is $h_c$=1.190 μm and the depth of grating groove is $h_g$=1.050 μm, the reflective efficiency of the ±1st orders and 0th order for TE polarization is 48.70% and 0.33%, respectively, where the total efficiency is 97.73%. Under TM polarized light wave, the efficiency of the ±1st orders is 48.39%, the efficiency in 0th order is 0.09%, and the total efficiency is 96.87%. When the thickness of $h_c$ is 1.190 μm and the depth of $h_g$ is between 1.000-1.150 μm, the efficiency in the ±1st orders is better than 47% for both TE and TM polarizations, and the efficiency of 0th order can be less than 0.7% and 3.5% under TE and TM polarizations, respectively. The data of the efficiency for the optimized grating are shown in Table 2.

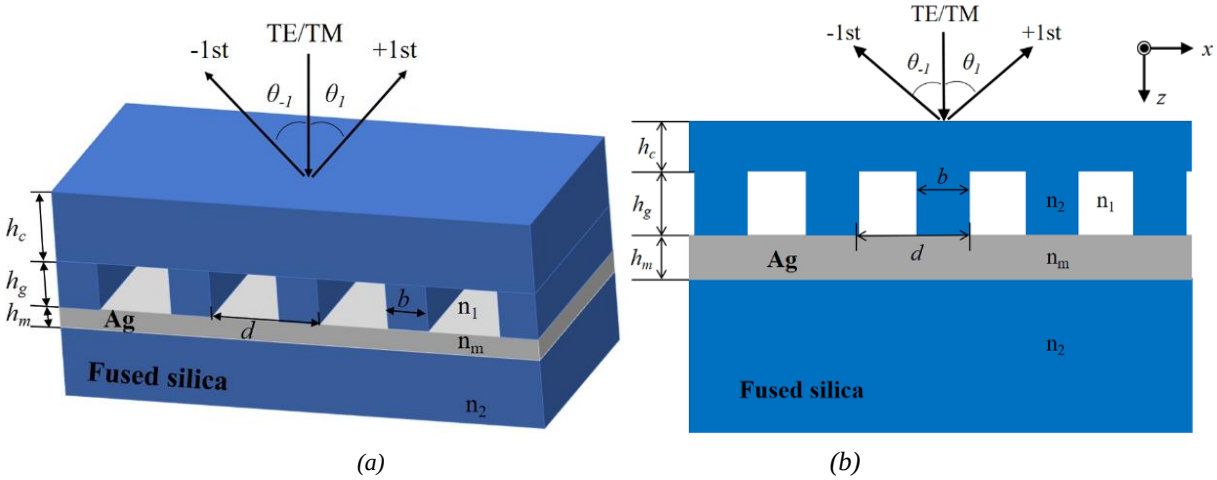


(a) (b)

*Fig. 1. Schematic of a two-port encapsulated grating under normal incidence: (a) 3-D view (b) 2-D view (color online)*

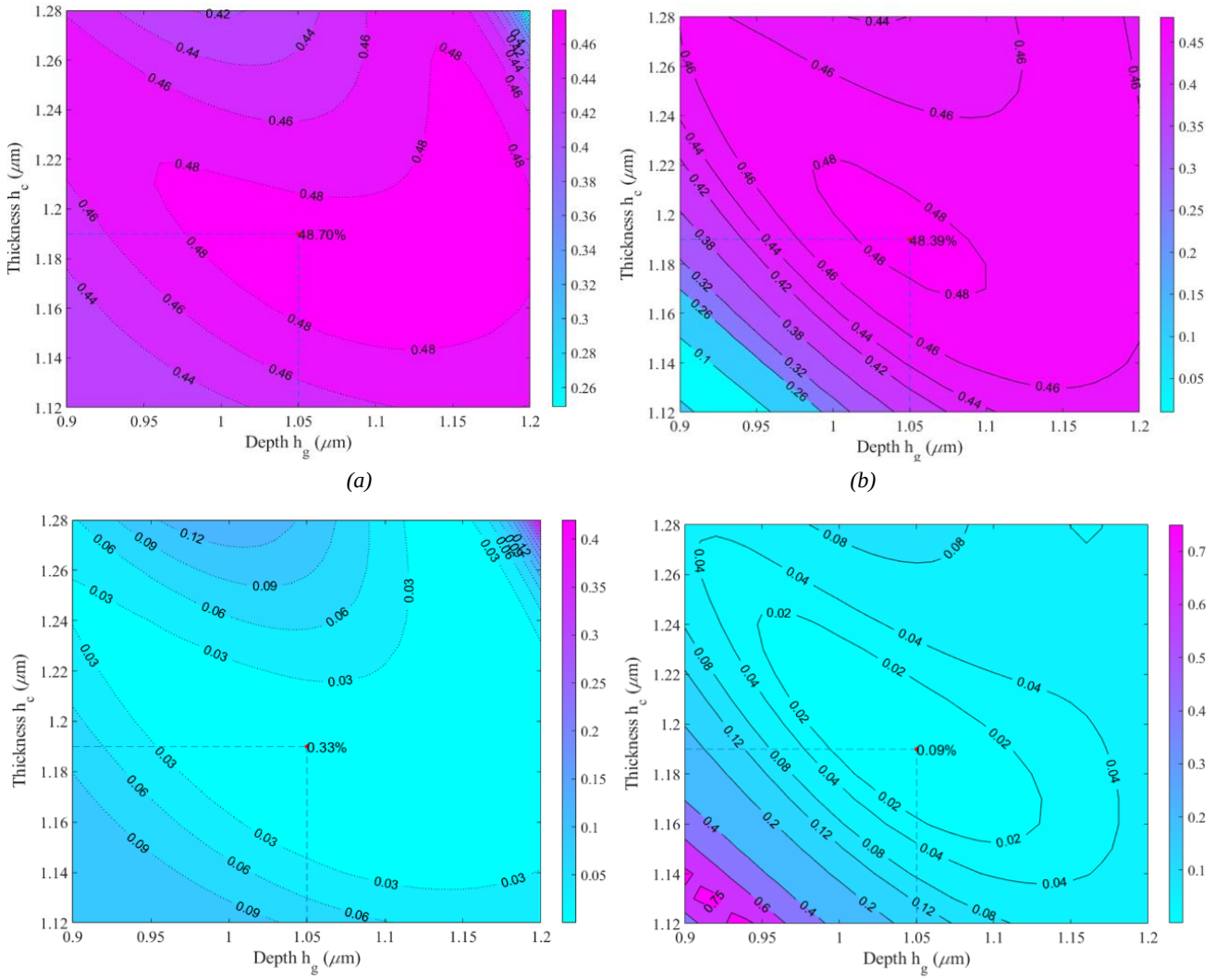


*Fig. 2. The reflection efficiency versus the thickness of the covering layer and the grating groove depth under normal incidence with λ=1.550 μm, d=2.954 μm, $h_m$=0.100 μm and f=0.43: (a) 1st order of TE polarization, (b) 1st order of TM polarization, (c) 0th order of TE polarization, (d) 0th order of TM polarization (color online)*

*Table 2. The efficiencies of two-port encapsulated grating with the optimized parameters based on RCWA and FEM*

| Calculation method | $\eta_0^{TE}$ (%) | $\eta_{\pm1}^{TE}$ (%) | $\eta_0^{TM}$ (%) | $\eta_{\pm1}^{TM}$ (%) |
|---|---|---|---|---|
| RCWA | 0.33% | 48.70% | 0.09% | 48.39% |
| FEM | 0.25% | 48.66% | 0.11% | 48.32% |

Compared with reported Refs. [26-28], the efficiencies of the ±1st orders for both TE and TM polarizations are significantly improved. Compared with reported Ref. [27], the suppression of the efficiency in 0th order under TM polarization is strengthened. Compared with reported Refs. [26, 28], the inhibition of the efficiency for 0th order is enhanced under TE and TM polarizations. The detailed comparative data are illustrated in Table 3.

*Table 3. Comparison of efficiencies between this work and reported Refs. [26-28]*

| Scheme | $\eta_0^{TE}$ (%) | $\eta_{\pm1}^{TE}$ (%) | $\eta_2^{TE}$ (%) | $\eta_0^{TM}$ (%) | $\eta_{\pm1}^{TM}$ (%) | $\eta_2^{TM}$ (%) |
|---|---|---|---|---|---|---|
| Ref. [26] | <1.3% | 46.15% | 1.16% | <1.3% | 43.60% | 4.29% |
| Ref. [27] | 0.21% | 48.36% | / | 0.23% | 48.34% | / |
| Ref. [28] | 0.51% | 48.01% | / | 0.85% | 47.90% | / |
| This work | 0.33% | 48.70% | / | 0.09% | 48.39% | / |

It is necessary to save resources and cost in actual manufacturing. Fig. 3 refers to the relationship between the

reflection efficiency and the thickness of the silver reflected layer under the optimized parameters. In Fig. 3, the reflection efficiency will increase with the increase of $h_m$ (between 0-0.100 μm). For $h_m$ of 0.100 μm, the reflection effect reaches the maximum. When $h_m$ is greater than 0.100 μm, the reflection efficiency hardly changes, which is the reason why $h_m$ is set to 0.100 μm.

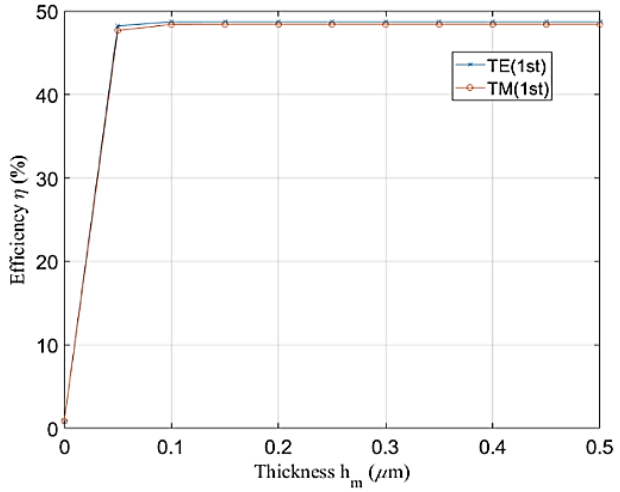


*Fig. 3. The relationship between the reflection efficiency and the thickness of silver reflector (color online)*

The distribution of electric field can help better understand the physical process of light propagation in the encapsulated grating. Fig. 4 shows the normalized electric field distribution of diagram for the beam splitting grating. From Fig. 4, it can be seen that almost all the energy of the light wave with a wavelength of 1550 nm under normal incidence condition is reflected back by the silver reflector, which is consistent with the results of RCWA. The energy distribution under either TE polarization or TM polarization presents discrete localization characteristics, and the propagation process of both incident and reflection is wavy along the Z-axis, which is caused by the normal incidence. However, the energy distribution structure and position will change with the polarization of the light source. Under the TE polarization, the energy is distributed at several maximum points, but under TM polarization, the maximum energy is mainly distributed in grating groove, which is just opposite to that under TE polarization.

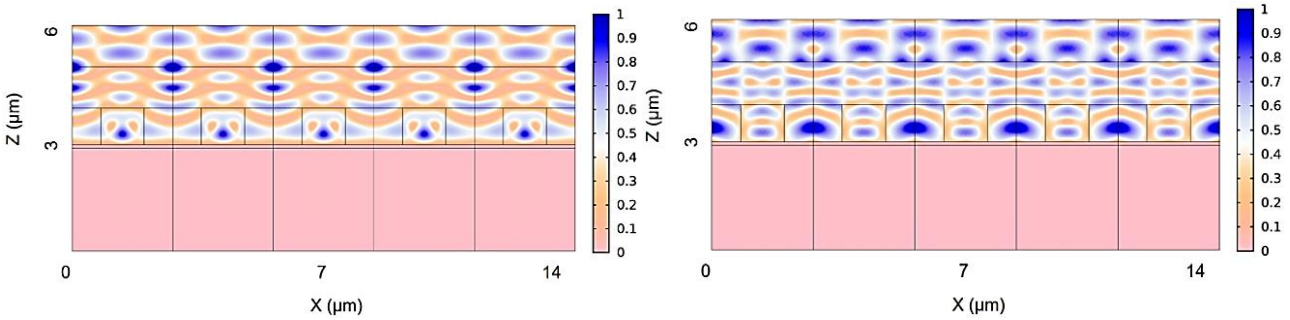


*(a)* *(b)*

*Fig. 4. Normalized electric field distribution diagram of the encapsulated grating under normal incidence: (a) TE polarization (b) TM polarization (color online)*

## 3. Analysis and discussions

Under normal incidence, the performance of the optimized grating can reach the best when the incident wavelength is 1550 nm. However, the wavelength will deviate from 1550 nm in actual use. Fig. 5 illustrates the efficiency of grating at different wavelengths. As shown in Fig. 5, the efficiency of the ±1st orders under both TE and TM polarizations can be greater than 47% when the wavelength is between 1532-1563 nm (the bandwidth is 31 nm).

The inhibition effect of the efficiency for 0th order is very nice in this wavelength range, with the efficiency of less than 3.6% for both TE and TM polarizations. Compared with reported Refs. [27, 28], the performance of bandwidth is greatly improved. The specific data are shown in Table 4. This shows that the proposed grating has high performance and high stability, which is of great significance and value in practical applications for some optical elements that need to adjust the wavelength size.

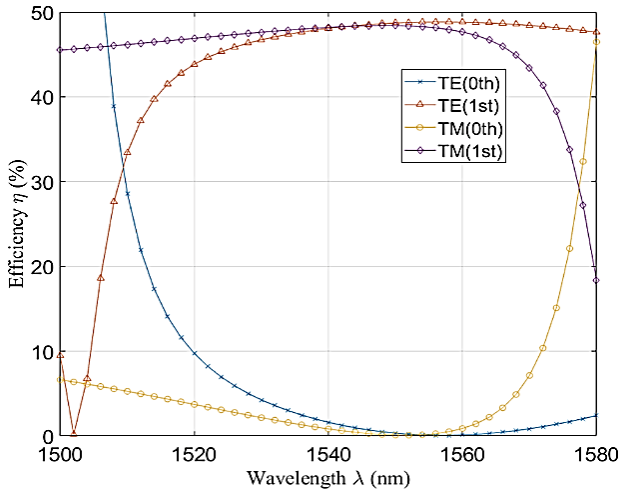


*Fig. 5. The relationship between efficiency and incident wavelength for both two polarizations under normal incidence with d=2.954 μm, f=0.43, $h_m$=0.100 μm, $h_c$= 1.190 μm and $h_g$=1.050 μm (color online)*

*Table 4. Comparison of bandwidth of wavelength between this work and reported Refs. [27, 28]*

| Scheme | $\eta_0^{TE/TM}$ (%) | $\eta_{\pm1}^{TE/TM}$ (%) | Bandwidth of wavelength |
|---|---|---|---|
| Ref. [27] | <5% | >46% | 1534-1557 nm (23 nm) |
| Ref. [28] | <2% | >47% | 1530-1550 nm (20 nm) |
| This work | <4% | >47% | 1532-1563 nm (31 nm) |

In theory, the period and duty cycle of the designed grating are certain, but this is difficult to achieve in practice. In some gratings, a slight change in grating period or duty cycle may cause a sharp decline in grating performance. Fig. 6 refers to the relationship between reflection efficiency and grating period under TE and TM polarizations. As illustrated in Fig. 6, when the grating period ranges from 2914 nm to 3015 nm, the efficiency of 0th order is less than 0.7% under TE polarization and less than 3.5% under TM polarization. The efficiencies of the ±1st orders for both TE and TM polarizations are both greater than 47%. The relationship between duty cycle and reflection efficiency is shown in Fig. 7. As shown in Fig. 7, under the duty cycle of 0.290-0.458, the efficiencies of the 0th order and ±1st orders for both TE and TM polarizations are less than 3.5% and better than 47%, respectively. Compared with reported Ref. [28], the fabrication tolerance of grating in this work is greatly improved. The specific data are shown in table 4. From the above analysis, it can be seen that the designed grating has a very large fabrication tolerance in period and duty cycle, which is very rare in previous reports. Therefore, the proposed grating is of great significance to many micro-nano optical elements and systems.

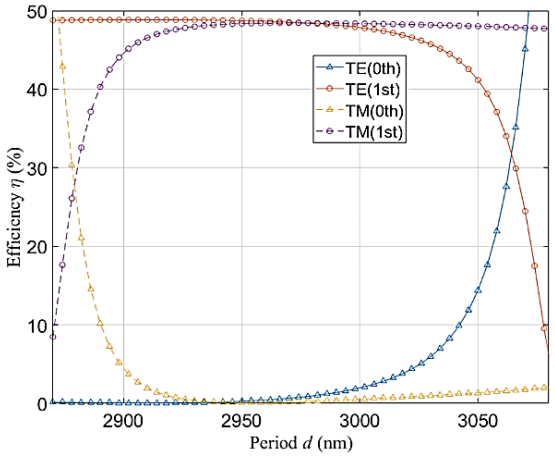


*Fig. 6. Reflection efficiency at different periods for both two polarizations under normal incidence with λ=1.550 μm, f=0.43, $h_m$=0.100 μm, $h_c$= 1.190 μm and $h_g$=1.050 μm (color online)*

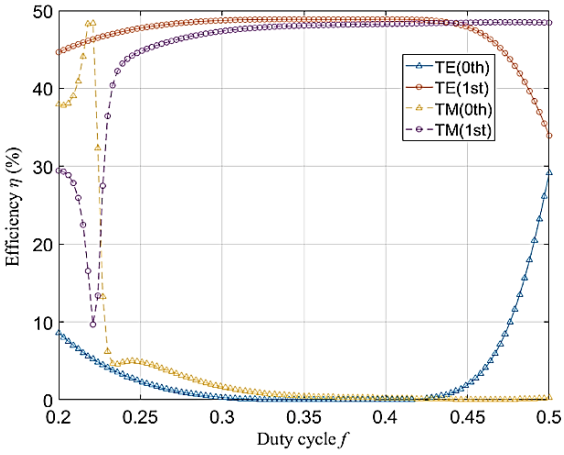


*Fig. 7. Reflection efficiency at different duty cycle for both two polarizations under normal incidence with the parameters of λ=1.550 μm, d=2.954 μm, $h_m$=0.100 μm, $h_c$= 1.190 μm and $h_g$=1.050 μm (color online)*

*Table 5. Comparison of fabrication tolerance between this work and reported Ref. [28]*

| Scheme | $\eta_0^{TE/TM}$ (%) | $\eta_{\pm1}^{TE/TM}$ (%) | Period | Duty cycle |
|---|---|---|---|---|
| Ref. [28] | / | >47% | 2965-2990 nm (25 nm) | 0.370-0.400 (0.030) |
| This work | <4% | >47% | 2914-3015 nm (101 nm) | 0.290-0.458(0.168) |

## 4. Conclusion

To summarize, a super-stability encapsulated grating with an incident wavelength of 1550 nm under normal incidence is simulated and optimized by RCWA, which has the characteristics of simple structure and low material cost. Unlike most reported two-port gratings, the proposed

encapsulated grating can realize high-efficiency output in ±1st orders with the inhibition of the zeroth order under TE and TM polarizations. The efficiency can less than 0.5% for 0th order under both TE and TM polarizations, and the efficiency of ±1st orders for TE and TM polarizations can achieve reach 48.70% and 48.39%, respectively. Furthermore, the analysis results show that the proposed grating not only has a wide wave bandwidth but also has a large fabrication tolerance, which is improvement compared with the previously reported. Hence, the proposed encapsulated grating has a broad application prospect in optical polarization devices, laser systems and polarization imaging, etc.

**Acknowledgements**

This work is supported by the Science and Technology Program of Guangzhou (202002030284, 202007010001, 202002030210) and the National Natural Science Foundation of China (62175039).

## References

[1] R. Arunkumar, J. K. Jayabarathan, S. Robinson, J. Optoelectron. Adv. M. **21**(7-8), 435 (2019).
[2] A. Aziz, Laser Phys. **30**(1), 016207 (2020).
[3] S. S. Mousavi Fard, A. H. Farhadian, M. Abbasabadi, Laser Phys. **30**(12), 126202 (2020).
[4] G. Wu, Y. Huang, X. Duan, K. Liu, X. Ma, T. Liu, H. Wang, X. Ren, Opt. Commun. **456**, 124458 (2020).
[5] E. ElShamla, S. Hekal, L. R. Gomaa, Opt. Commun. **457**, 124621 (2020).
[6] Z. Xu, T. Lyu, X. Sun, Opt. Commun. **451**, 17 (2019).
[7] X. Liang, X. Zhang, Y. Chen, Y. Zhang, Optik **202**, 163557 (2020).
[8] Y. Liu, X. Zhang, Y. Huang, J. Zhang, W. Hofmann, Y. Ning, L. Wang, Optik **183**, 579 (2019).
[9] J. Cheng, Z. Yang, Laser Phys. **30**(7), 075105 (2020).
[10] L. Liu, Y. Li, X. Li, Opt. Commun. **458**, 124810 (2020).
[11] X. Yuan, S. Feng, S. Nie, C. Chang, J. Ma, C. Yuan, Opt. Commun. **431**, 126 (2019).
[12] A. J. Christy, A. Umamakeswari, Optik **218**, 164953 (2020).
[13] Y. Zheng, B. Xia, L. Jiang, X. Wu, J. Duan, Optik **217**, 164890 (2020).
[14] M. A. Butt, S. N. Khonina, N. L. Kazanskiy, Laser Phys. **30**(1), 016201 (2020).
[15] F.-Q. Dou, Z.-M. Yan, X.-Q. Liu, W.-Y. Wang, C.-C. Shu, Optik **210**, 164516 (2020).
[16] J. Chen, D. Gao, Optik **220**, 165131 (2020).
[17] N. Fouad, M. Badr, M. Fedawy, M. Swillam, Opt. Commun. **474**, 126098 (2020).
[18] I. S. Amiri, A. N. Z. Rashed, H. M. A. Kader, A. A. Al-Awamry, I. A. Abd El-Aziz, P. Yupapin, G. Palai, Optik **207**, 163853 (2020).
[19] B. Gong, H. Wen, H. Li, IEEE Photon. J. **12**(2), 6500208 (2020).
[20] Z. Yin, J. Yu, Y. Lu, C. Zhou, IEEE Photon. Technol. Lett. **32**(6), 309 (2020).
[21] W. Zhu, B. Wang, C. Fu, J. Fang, Laser Phys. **30**(6), 066201 (2020).
[22] C. Gao, B. Wang, C. Fu, J. Fang, K. Wen, Z. Meng, Z. Nie, L. Chen, L. Lei, J. Zhou, J. Optoelectron. Adv. M. **21**(7-8), 429 (2019).
[23] S. Li, C. Zhou, H. Cao, J. Wu, Opt. Lett. **39**(4), 781 (2014).
[24] H. Li, B. Wang, Sci. Rep. **7**, 1309 (2017).
[25] J. Feng, C. Zhou, J. Zheng, H. Cao, P. Lv, Appl. Opt. **48**(14), 2697 (2009).
[26] B. Wang, Sci. Rep. **5**, 16501 (2015).
[27] B. Wang, IEEE Photon. J. **8**(1), 7801706 (2016).
[28] C. Fu, B. Wang, J. Fang, K. Wen, Z. Meng, Q. Wang, Z. Nie, X. Xing, L. Chen, L. Lei, J. Zhou, Optoelectron. Adv. Mat. **14**(7-8), 297 (2020).
[29] Z. Yin, Y. Lu, J. Yu, C. Zhou, Chin. Opt. Lett. **18**(7), 070501 (2020).
[30] Q. Zhao, W. Yu, Y. Zhao, S. Dai, J. Liu, Opt. Commun. **475**, 126282 (2020).
[31] M. G. Moharam, D. A. Pommet, E. B. Grann, T. K. Gaylord, J. Opt. Soc. Am. A **12**(5), 1077 (1995).
[32] L. Qian, K. Wang, W. Zhu, C. Han, C. Yan, Opt. Commun. **452**, 273 (2019).

*Corresponding author: wangb_wsx@yeah.net